

International Conference on Space Optics—ICSO 2014

La Caleta, Tenerife, Canary Islands

7–10 October 2014

Edited by Zoran Sodnik, Bruno Cugny, and Nikos Karafolas



Monolithic master oscillator power amplifier at 1.58 μm for lidar measurements

M. Faugeron

M. Krakowski

Y. Robert

E. Vinet

et al.



icso proceedings



MONOLITHIC MASTER OSCILLATOR POWER AMPLIFIER AT 1.58 μM FOR LIDAR MEASUREMENTS

M. Faugeron^{1*}, M. Krakowski¹, Y. Robert¹, E. Vinet¹, P. Primiani¹, J. P. Le Goëc¹, O. Parillaud¹, F. van Dijk¹, M. Vilera², A. Consoli², J. M. G. Tijero², I. Esquivias²

¹*III-V Lab, a joint Laboratory of "Alcatel Lucent Bell Labs", "Thales Research & Technology" and "CEA-LETI", Campus Polytechnique, 1, Avenue A. Fresnel, 91767 Palaiseau cedex, France,*

²*Universidad Politécnica de Madrid, ETSI Telecomunicación-CEMDATIC, Avda. Complutense 22, 28040 Madrid, Spain*

**Mickael Faugeron, Tel: + 33 (0) 1 69 41 58 10, e-mail: mickael.faugeron@3-5lab.fr*

I. INTRODUCTION

Nowadays the interest in high power semiconductor devices is growing for applications such as telemetry, lidar system or free space communications. Indeed semiconductor devices can be an alternative to solid state lasers because they are more compact and less power consuming. These characteristics are very important for constrained and/or low power supply environment such as airplanes or satellites.

Lots of work has been done in the 800-1200 nm range for integrated and free space Master Oscillator Power Amplifier (MOPA) [1]-[3]. At 1.5 μm , the only commercially available MOPA is from QPC [4]: the fibred output power is about 700 mW and the optical linewidth is 500 kHz.

In this paper, we first report on the simulations we have done to determine the appropriate vertical structure and architecture for a good MOPA at 1.58 μm (section II). Then we describe the fabrication of the devices (section III). Finally we report on the optical and electrical measurements we have done for various devices (section IV).

II. DEVICES SIMULATIONS

A. MOPA architecture

A MOPA is composed at least by a laser and an amplification section. In the framework of the FP7-Space Britespace project we have to develop an integrated MOPA composed of a distributed feedback laser (DFB), a modulation section and a semiconductor optical amplifier (SOA) [5]. The DFB laser is the natural candidate to obtain a single-mode emission laser with a narrow optical linewidth. In the past, we have already developed DFB lasers which exhibit high output power (> 150 mW) with an optical linewidth better than 300 kHz [6].

The modulation section has to allow a modulation bandwidth about 15 Mbit/s with 10 dB extinction ratio. A simple way is to use gain modulation in a SOA. Compared with electro-absorption modulator (EAM), which requires a specific material (photoluminescence peak shifted compared with the laser active zone), we do not need any specific active zone for the SOA.

The MOPA maximum output power will be given by the saturation power of the SOA. In order to obtain an output power as large as possible, we have decided to use a flared SOA. Indeed the active zone enlargement allows decreasing the power density and increasing the maximum output power [7].

The standard configuration for a monolithic MOPA is to integrate the different sections in straight line (Fig. 1(a)) [4], [8]. The main advantage of this architecture is its simplicity. The main drawbacks are the reflections at the facets (even with appropriate antireflective coatings) or at the interfaces between integrated elements which can produce multicavity effects, disturbance of the DFB laser due to large reflections or lasing effect in each section. The impact of these reflections on the power or the optical spectrum is described in [8].

In order to decrease the reflections at the facets, a simple method consists in tilting the device with regard to the facets (Fig. 1(b)) [9]. This technique is very common for SOAs. The main drawback is the difficulty to make efficient high reflective coatings on the backside DFB laser facet due to the tilt.

Another promising architecture is the bended MOPA (Fig. 1(c)) [10]. For our 3 sections MOPA, the DFB laser is straight, the modulation section is bended and the flared SOA is tilted. This architecture seems ideal because it allows reducing the reflections at the SOA facet thank to the SOA tilt and the backside DFB facet coatings can be well controlled. The main uncertainty concerns the losses due to the bend.

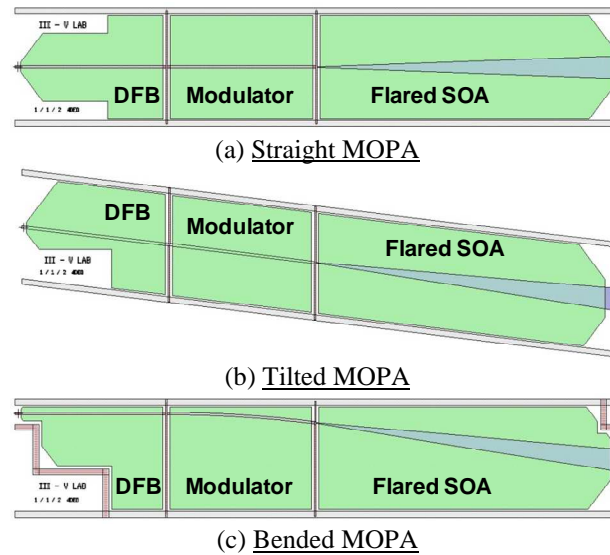


Fig. 1. Three architectures: straight MOPA (a), tilted MOPA (b) and bended MOPA (c).

B. Eigenmode of the cavity

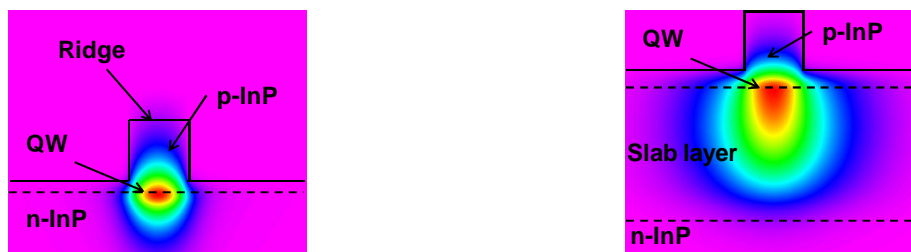
At $1.55 \mu\text{m}$ the main losses in an Indium Phosphide (InP) semiconductor structure are due to the intervalence band absorption (IVBA) in the p-doped layers. To enhance the optical power it is necessary to decrease the confinement, which is the overlap between the optical mode and a given surface, with the lossy p-doped layers. An innovative approach developed by the MIT Lincoln Lab at various emission wavelengths, consists in using an asymmetrical cladding structure [7]: a large slab inserted between the active zone and the substrate allows attracting the optical mode and taking it away from the p-doped layers. They have called this structure SCOW for Slab Coupled Optical Waveguide. The slab optical index has to be between the active zone index and the substrate index. Fig. 2(a) shows the optical eigenmode of an InP semiconductor cavity with a standard vertical structure. The optical mode is centered on the quantum wells (QWs), represented by the dashed line, and equally spread between the p-doped and the n-doped InP layers. Fig. 2(b) shows the optical eigenmode of a cavity with a slab layer structure (asymmetrical cladding structure). In this case, the optical mode is not centered on the active zone but below the active zone. The optical mode is mainly spread on the n-doped slab and only a little part of the mode is on the p-doped layers.

The corresponding optical parameters simulated with homemade software which calculates the optical eigenmode are given in the Tab. 1. We clearly see the impact of the $2 \mu\text{m}$ thick slab: the confinement on the QWs (Γ_{QW}) is divided by 3.5 and the confinement on the p-doped InP ($\Gamma_{\text{p-InP}}$) by almost 6. The large overlap reduction with the p-doped layers is responsible for the optical losses decrease. The QWs confinement decrease will lead to a reduction of the structure modal gain: it will be necessary both to ensure an adequate overlap with the QWs during the cavity simulation stage to maintain enough modal gain and to use long cavities. The asymmetrical cladding structure allows enlarging the optical eigenmode: we can see this effect on the vertical divergence (Tab. 1). This point is very important because a large optical mode is equivalent to an optical beam with a low divergence which is in favour of a better coupling efficiency.

For the asymmetrical cladding structure, the choice of the slab material is very important because it sets the optical index of the slab. We see in Fig. 3 the strong impact on the cavity eigenmode for a variation of the slab optical index. For a slab optical index of 3.20, the eigenmode is centered on the active zone and the slab has a small impact on the eigenmode (Fig. 3(a)). When the slab index is increased to 3.25, the eigenmode is enlarged and strongly deformed by the slab (Fig. 3(b)). For a higher slab optical index ($n = 3.31$), the eigenmode is centered in the slab layer and the optical mode is not well confined (Fig. 3(c)).

The slab optical index needs to be between the active zone index ($n_{\text{AZ}} \approx 3.5$) and the substrate ($n_{\text{InP}} = 3.16$). There are two possibilities for the slab realization. The first one, which is the most intuitive, is to use a bulk or massive material with the appropriate optical index. It can be for example an InGaAsP material with the appropriate photoluminescence peak [7], [11]. All the eigenmode simulations plotted in Fig. 2 and 3 have been done for structures with massive slab. The drawback of this solution is that we need to develop in epitaxy a specific material with the required optical index, for example an InGaAsP quaternary, which leads to lots of epitaxy calibrations and testing. Another drawback is that the quaternary material has bad thermal conductivity behaviour which can be an issue for high power devices. The second option is to replace the bulk material by a “dilute” material [6]. A dilute material is composed of thin layers of various materials (typically two materials): the optical index of the dilute material is the average of the various material indexes weighted by their thickness

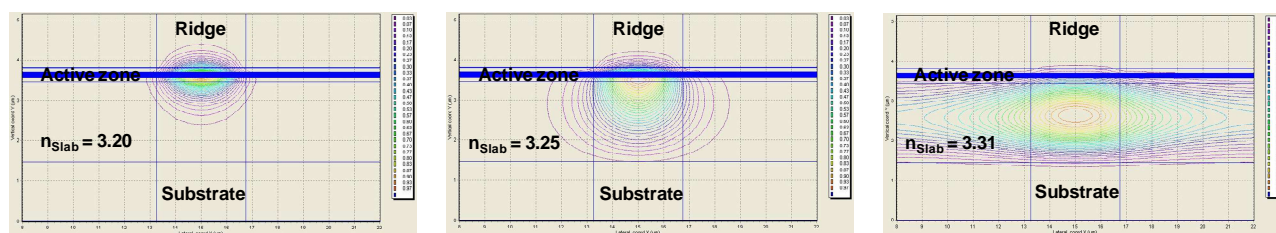
(Fig. 4(a)). The interest of this solution is that we can use standard material such as InP and the barrier material to make the slab layer: it is not necessary to develop any quaternary materials. We can also modify the slab index by modifying the relative thickness of the layers. It leads to more degrees of freedom for the design of the vertical structure. This point is demonstrated in Fig. 4(b) and (c) where we have plotted the optical eigenmode for 2 structures with the same total slab thickness but with different relative thicknesses of the InP and the InGaAsP. In Fig. 4(b), for a given structure, the mode is centered just below the active zone. In Fig. 4(c), we have maintained the total slab thickness but we have increased the thicknesses of the InGaAsP layers and we have decreased the thicknesses of the InP layers. This leads to an increase of the average slab optical index because the index of the InGaAsP is higher than the InP. We can notice that the eigenmode has moved to the bottom and is now centered in the middle of the slab because it is attracted by the higher slab index.



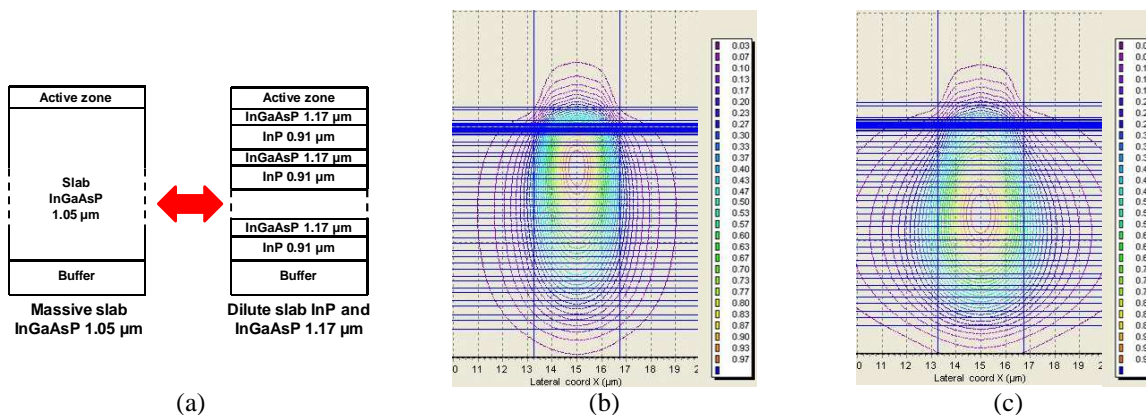
(a) No slab (typical epitaxial structure) (b) 2 μm thick slab
Fig. 2. Optical eigenmode for structures without slab (a), and with a 2 μm thick slab.

Tab. 1. Simulated optical parameters for a standard structure and an asymmetrical cladding structure.

Parameters	Standard structure	Asymmetrical cladding structure
Γ_{QW}	7.5 %	2.1 %
Γ_{p-InP}	31.7 %	5.6 %
Estimated optical losses	12.5 cm ⁻¹	3.6 cm ⁻¹
Vertical divergence (FWHM)	34.6°	29.2°



(a) $n_{slab} = 3.20$ (b) $n_{slab} = 3.25$ (c) $n_{slab} = 3.31$
Fig. 3. Optical eigenmode for asymmetrical cladding with 3 different slab materials.



(a) (b) (c)
Fig. 4. Principle of a dilute slab (a). Optical eigenmodes for 2 epitaxial structures with the same total slab thickness but different InP/InGaAsP thicknesses (b), (c).

C. Bend simulation

In the bended MOPA architecture, the modulation section makes the transition between the straight DFB laser and the tilted SOA. The modulator curvature radius is determined by the length of the section and the tilt of the next section (flared SOA) which is set to 7° . It is difficult to directly simulate a bend because the output of the bend is tilted compared with the input of the bend. A useful method consists in simulating a S-bend (2 bend head to foot): in that case there is no tilt between the input and the output. We have simulated the propagation losses due to the S-bend for various section lengths by using the Beamprop software. The results are summarized in Tab. 2 and Fig. 5. The launched mode is the eigenmode of the straight section. For each configuration, the simulation on the left represents the propagation of the optical mode in the XZ plane (the Y position is the active zone). The curve on the right is the overlap between the propagated mode and the launched eigenmode.

Fig. 5(a) is a plot of the simulation of the eigenmode propagation in a 1 mm long straight section. The propagation is without any propagation losses, which means that our eigenmode calculation is correct. Fig. 5(b)-(d) are the plots for the S-bends with various lengths (1.0, 1.4 and 2.0 mm). For the 1 mm long S-bend the losses are significant (-4.56 dB): we can see on the Fig. 5(b) the optical power leakage along the bend. For the 2 mm long S-bend, we have obtained optical losses lower than 1 dB (Fig. 5(d)). In the bended MOPA architecture we just have half a S-bend. With a 1 mm long bended modulator, the propagation losses should be around 0.5 dB. We will use this length for our MOPA.

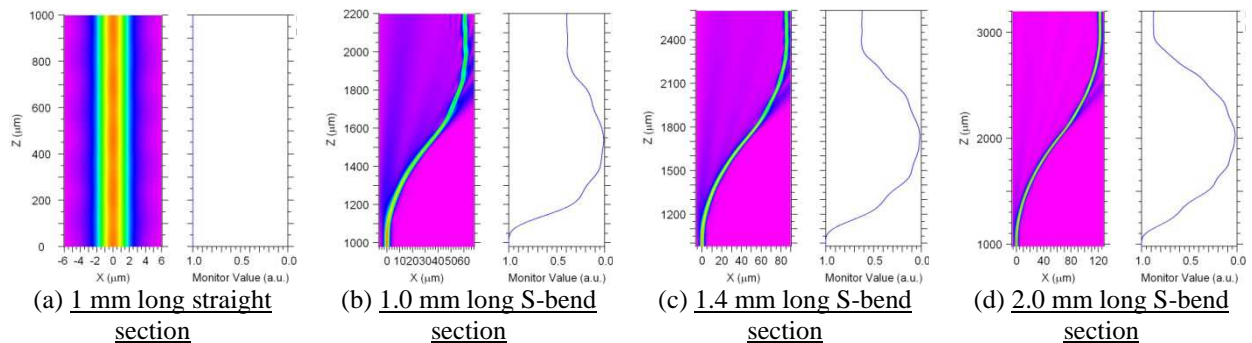


Fig. 5. Propagation of the optical eigenmode on a straight section (a) and S-bend with various lengths: 1 mm (b), 1.4 mm (c) and 2 mm (d).

Tab. 2. Propagation transmission and losses for various S-bend lengths.

S-bend length (mm)	Radius of curvature (mm)	Transmission (%)	Losses (dB)
1	4.1	35	-4.56
1.4	5.7	62	-2.07
2	8.2	86	-0.66
3	12.3	94	-0.27

III. ELECTED STRUCTURE AND DEVICES FABRICATION

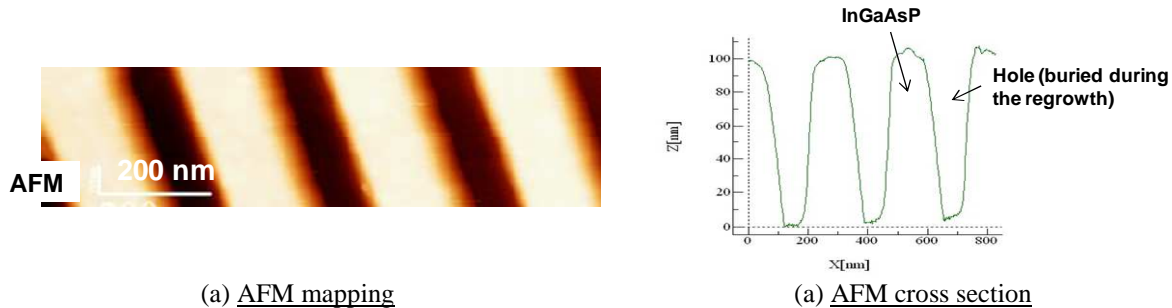
A. Elected design

We have designed our asymmetrical cladding structure using a dilute slab composed of InP and InGaAsP ($\lambda_g = 1.17 \mu\text{m}$) in order to avoid any material development. Indeed this quaternary material is the same as the barrier material. The slab thickness ($1.62 \mu\text{m}$) has been optimized to decrease the optical confinement within the p-doped layers as much as possible and to maintain the confinement within the QWs around 2%. This level of confinement is necessary to maintain a low threshold current, a low RIN and a quite large relaxation frequency.

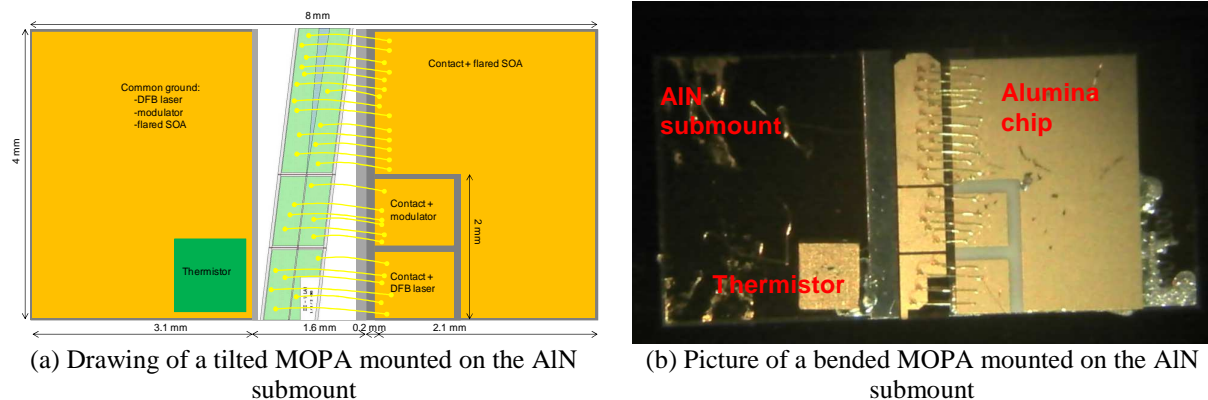
B. MOPA architecture

The multiple quantum wells DFB structure was grown by Metal Organic Vapor Phase Epitaxy (MOVPE) on n-type InP substrates. The active region contains six 8 nm thick compressively (0.85%) strained InGaAsP quantum wells and five 10 nm thick InGaAsP ($\lambda_g = 1.17 \mu\text{m}$) barriers. The photoluminescence peak was at $1.57 \mu\text{m}$. After a first epitaxy, first order gratings were defined by e-beam lithography and inductively coupled plasma (ICP) reactive ion etching. An atomic force microscope (AFM) image of the grating after ICP etching is plotted in Fig. 6. The InGaAsP grating layer is positioned above the active zone and the grating layer thickness is optimized in order to obtain a coupling strength $KL \sim 1.4$. This low value of KL should limit spatial hole

burning effects and the associated optical power saturation. Re-growth of p-doped top cladding was then also done by MOVPE. The dual-channel ridge-waveguide used for the DFB laser and the modulator section was formed by ion beam etching followed by wet chemical etch and proton insulation. The ridge-waveguides are 3.0 μm wide. This value was found to minimize the thermal saturation while preserving lateral single-mode operation. A 4 μm thick gold layer is deposited on the surface as heatsink and to allow electrical bonding in safer conditions. Bars were cleaved to form 4 and 5 mm long devices. Facets were high reflectivity (HR) coated on the DFB laser backside facet and anti reflectivity (AR) coated on the SOA facet. Chips cleaved from the bars were mounted p-side up on aluminum nitride (AlN) submounts. A thermistor was glued on the submount to better control the chip temperature. A drawing of a tilted MOPA soldered on the AlN submount is shown in Fig. 7(a). Fig. 7(b) is a picture of a bended MOPA mounted on the AlN submount.



(a) AFM mapping
Fig. 6. AFM measurements on the Bragg grating before the epitaxial regrowth.
(a) AFM cross section



(a) Drawing of a tilted MOPA mounted on the AlN submount
(b) Picture of a bended MOPA mounted on the AlN submount
Fig. 7. MOPA mounted on AlN submount.

IV. DEVICE CHARACTERIZATION

All the MOPA measurements have been done on devices mounted on AlN submounts. The current was injected through electrical probes for the DFB laser and the modulator and through large metallic stripes for the flared SOA in order to reduce the electrical resistance and to allow high current values. The submount temperature was controlled thanks to the thermistor glued on the submount. All the measurements have been performed at 18° C.

The tilted MOPAs are not operational, because the DFB laser is not lasing. In the following sections, we will focus on the straight and bended MOPAs.

A. Straight MOPA

We have first tested the straight MOPAs. Even if we have obtained hundreds of mW at the output of the device, we have rapidly seen the drawbacks of this architecture. First we have observed multimode behavior on the optical spectrum: for example in Fig. 8(a) we can see some peaks around 1582 nm (grating wavelength) and also some optical modes around 1595 nm. This multimode behavior, which is varying as a function of the current on the different sections, is not recommended for system applications. For some triplets of current (DFB laser, modulator and flared SOA) the optical spectrum seems single-mode but when we characterize electrically the signal we see some peaks at different frequencies (Fig. 8(b)). These peaks are the beatings between optical modes. In Fig. 8(b), we have the fundamental tone between 5 and 6 GHz and the 2nd and 3rd harmonics. The frequency beatings change when the DFB current is changed.

As expected, the straight architecture is not relevant due to instability in the optical spectrum. These instabilities make the use of the device in a lidar system not possible.

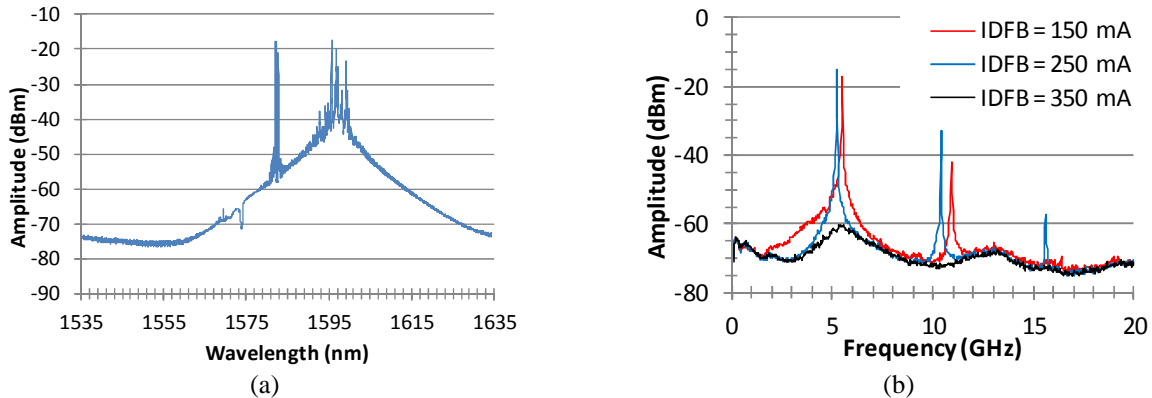


Fig. 8. Optical spectrum (a) and electrical spectrum for a straight MOPA (b).

B. Bended MOPA

We have then characterized bended MOPAs. For a 4 mm long MOPA (1 mm DFB laser, 1 mm modulator and 2 mm flared SOA) the maximum output power is about 430 mW for bias currents of 400 mA in the laser, 300 mA in the modulator and 3 A in the flared SOA (Fig. 9(a)). The corresponding optical spectrum is plotted in Fig. 9(b). The side mode suppression ratio (SMSR) is superior to 45 dB. The output power is limited by the flared SOA thermal saturation. This saturation appears at low current density (2 kA.cm^{-2}) compared with similar structures such as [10] (4.64 kA.cm^{-2}). We think that this limitation is due to fabrication issue during the p-side contact annealing.

The optical spectrum for various flared SOA bias currents is plotted in Fig. 10(a). We have observed very stable single-mode operation when varying the flared SOA and the modulator bias currents. We do not see fluctuations of the wavelength due to reflections. Fig. 10(b) is the comparison of the optical spectrum from the DFB laser backside facet (DFB facet, blue curve) and from the flared SOA output facet (SOA facet, red curve). The shape of the curves is the same, the flared SOA just acts as an amplifier and does not modify the peak wavelength.

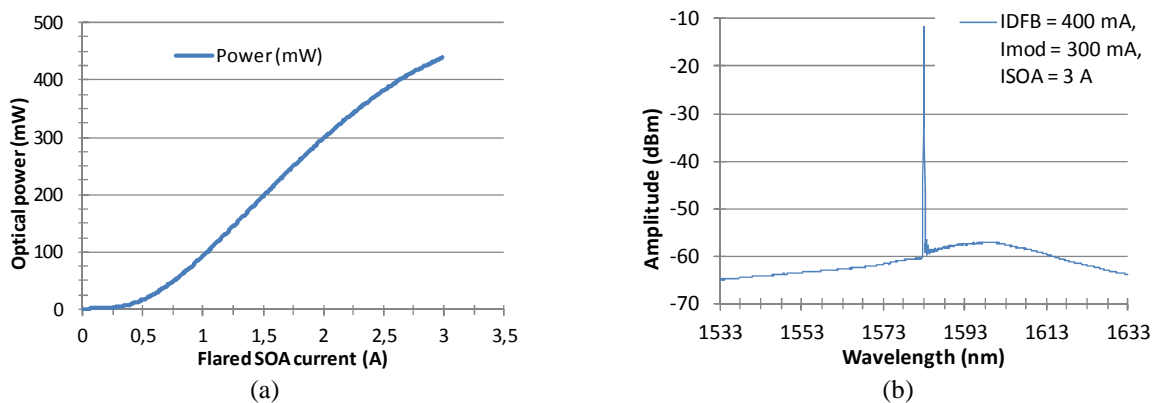


Fig. 9. Power as a function of the flared SOA current (a) and optical spectrum (b) for a bended MOPA.

The optical linewidth is an important parameter for some applications such as coherent lidar or free space communications. We use the delayed self-heterodyne method with 1 km SMF length to characterize our device and a low noise current source for the laser bias current. The optical linewidth is fitted with a Lorentzian curve: the FWHM extracted value represents the intrinsic linewidth of the DFB laser [6]. The linewidth as a function of the DFB laser current has been investigated (Fig. 11(a)) for a 5 mm long device (1 mm DFB laser, 1 mm modulator and 3 mm flared SOA). As for single DFB, the optical linewidth decreases when the DFB current increases. The photon density increase in the laser cavity when the bias current is increased is responsible for the optical linewidth reduction (the linewidth is inversely proportional to the photon density). Fig 11(b) is the evolution of the optical linewidth for various flared SOA currents.

We have measured the relative intensity noise (RIN) of the same bended MOPA from 0.1 to 40 GHz (Fig. 12(a)). The relaxation frequency remains inferior to 5 GHz even at high DFB bias current. Fig. 12(b) is a

comparison of the RIN measured at the DFB laser backside facet (straight lines) and at the SOA output facet (dashed lines). The position and the level of the relaxation frequency are the same.

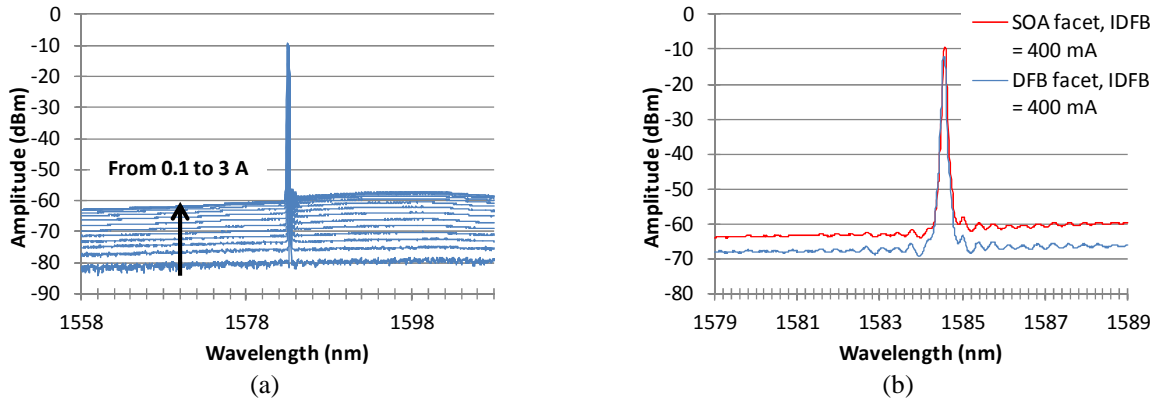


Fig. 10. Optical spectrum for different flared SOA current (a) and optical spectrum from both facets (b) for a bended MOPA.

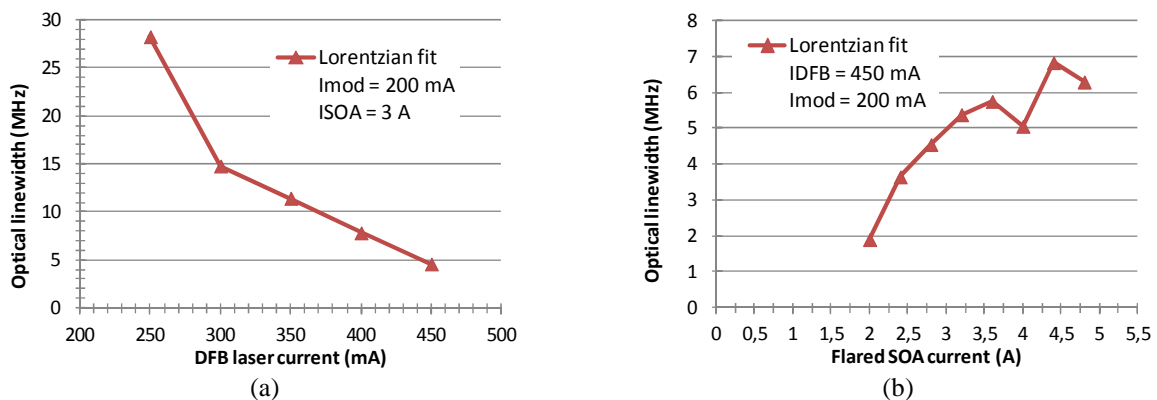


Fig. 11. Optical linewidth as a function of the DFB laser current (a) and the flared SOA current (b).

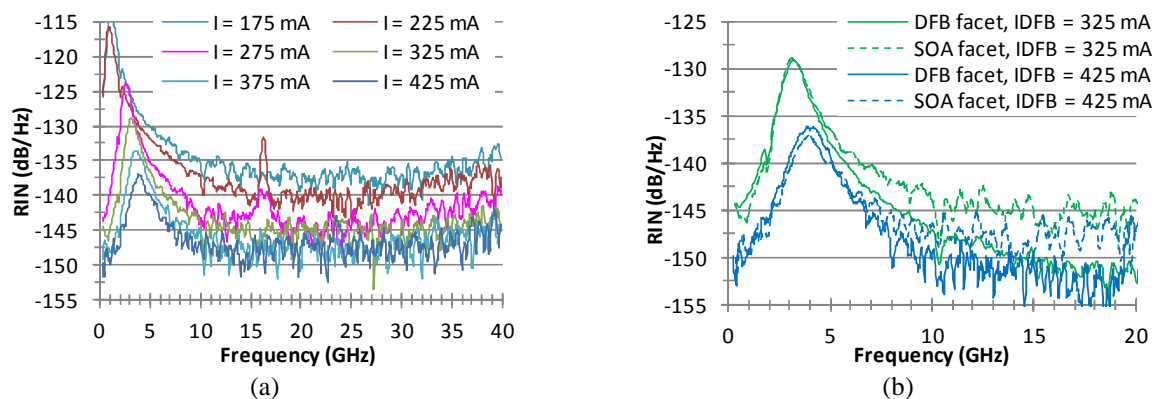


Fig. 12. RIN as a function of the DFB laser current (a) and RIN from both facets (b).

V. SUMMARY

In this paper, we report the design, the fabrication and the characterization of a monolithic semiconductor MOPA device at 1.58 μm . The objective was to develop a 3 sections device including a DFB laser, a modulation section and a high power amplifier. We have designed and fabricated 3 architectures: straight, tilted and bended. The bended and the straight architectures have been characterized and compared.

The straight MOPA suffers from optical spectrum instabilities most likely due to reflections at the facets and at the section interfaces. These components are not suitable for systems such as lidar where a very stable peak wavelength is required. We have performed more complete characterizations on bended MOPAs. The wavelength stability is largely enhanced thanks to the reduction of the optical feedback. We have demonstrated more than 400 mW output power at 1.58 μm with a SMSR superior to 45 dB. The main limitation for having

much power seems due to a bad ohmic contact in the fabrication which leads to a reduction of the reachable current density. We have obtained optical linewidth of about 5 MHz at FWHM which is compatible with our application of CO₂ detection lidar.

ACKNOWLEDGEMENT

This project has received funding from the European Union's Seventh Framework Programme for research technological development and demonstration under grant agreement no. 313200.

REFERENCES

- [1] S. O'Brien, R. Lang, R. Parke, J. Major, D. F. Welch, and D. Mehuys, "2.2-W Continuous-Wave Diffraction-Limited Monolithically Integrated Master Oscillator Power Amplifier at 854 nm," *IEEE Photon. Technol. Lett.*, vol. 9, no. 9, pp. 440-442, Apr., 1997.
- [2] S. O'Brien, A. Schoenfelder, and R. J. Lang, "5-W CW Diffraction-Limited InGaAs Broad-Area Flared Amplifier at 970 nm," *IEEE Photon. Technol. Lett.*, vol. 9, no. 9, pp. 1217-1219, Sep., 1997.
- [3] S. Spießberger, M. Schiemangk, A. Sahm, A. Wicht, H. Wenzel, A. Peters, G. Erbert, and G. Tränkle, "Micro-integrated 1 Watt semiconductor laser system with a linewidth of 3.6 kHz," *Opt. Express.*, vol. 19, no. 8, pp. 7077-7083, Apr. 2011.
- [4] M. L. Osowski, Y. Gewirtz, R. M. Lammert, S. W. Oh, C. Panja, V. C. Elarde, L. Vaissié, F. D. Patel, and J. E. Ungar, "High-power semiconductor lasers at eye-safe wavelengths," in *proc. SPIE 7325*, Laser Technology for Defense and Security V, paper 73250V, May, 2009.
- [5] I. Esquivias, A. Pérez-Serrano, J. M. G. Tijero, M. Faugeron, F. van Dijk, M. Krakowski, G. Kochem, M. Traub, J. Barbero, P. Adamiec, X. Ai, J. Rarity, M. Quatrevalet, and G. Ehret, "Random-modulation CW lidar system for space-borne carbon dioxide remote sensing based on a high-Brightness semiconductor Laser," in *proc. ICSO 2014*, International Conference on Space Optics, paper 66861, October, 2014.
- [6] M. Faugeron, M. Tran, O. Parillaud, M. Chtioui, Y. Robert, E. Vinet, A. Enard, J. Jacquet, and F. Van Dijk, "High-Power Tunable Dilute Mode DFB Laser With Low RIN and Narrow Linewidth," *IEEE Photon. Technol. Lett.*, vol. 25, no. 1, pp. 7-10, Jan, 2013.
- [7] P. W. Juodawlkis, J. J. Plant, W. Loh, L. J. Missaggia, F. J. O'Donnell, D. C. Oakley, A. Napoleone, J. Klamkin, J. T. Gopinath, D. J. Ripin, S. Gee, P. J. Delfyett, and J. P. Donnelly, "High-Power, Low-Noise 1.5- μ m Slab-Coupled Optical Waveguide (SCOW) Emitters: Physics, Devices, and Applications," *IEEE J. Sel. Top. Quantum Electron.*, vol. 17, no. 6, pp. 1698-1714, Nov/Dec. 2011.
- [8] M. Spreemann, M. Lichtner, M. Radziunas, U. Bandelow, and H. Wenzel, "Measurement and Simulation of Distributed-Feedback Tapered Master-Oscillator Power Amplifiers," *IEEE J. Quantum Electron.*, vol. 45, no. 6, pp. 609-616, June, 2009.
- [9] P. A. Yazaki, K. Komori, G. Bendelli, S. Arai, and Y. Suematsu, "A GaInAsP/InP Tapered-Waveguide Semiconductor Laser Amplifier Integrated with a 1.5 μ m Distributed Feedback Laser," *IEEE Photon. Technol. Lett.*, vol. 3, no. 12, pp. 1060-1063, Dec., 1991.
- [10] L. Hou, M. Haji, J. Akbar, and J. H. Marsh, "Narrow linewidth laterally coupled 1.55 μ m AlGaInAs/InP distributed feedback lasers integrated with a curved tapered semiconductor optical amplifier," *Opt. Lett.*, vol. 37, no. 21, pp. 4525-4527, Nov., 2012.
- [11] M. Faugeron, F. Lelarge, M. Tran, Y. Robert, E. Vinet, A. Enard, J. Jacquet, and F. Van Dijk, "High Peak Power, Narrow RF Linewidth Asymmetrical Cladding Quantum-Dash Mode-Locked Lasers," *IEEE J. Sel. Topics Quantum Electron.*, vol. 19, no. 4, pp. 1101008, July-Aug, 2013.